Capillary Entrapment Caused by Small-Scale Wettability Heterogeneities

P.P. van Lingen, SPE, **Johannes Bruining**, SPE, and **C.P.J.W. van Kruijsdijk**, SPE, Delft U. of Technology, Center for Technical Geoscience

Summary

Small-scale heterogeneities are abundant in oil reservoirs. It is well known that these heterogeneities can reduce the displacement efficiency of immiscible flooding because of capillary entrapment of oil. A typical heterogeneous facies is the laminated crossbed set with alternating high- and low-permeability laminae. Apart from this heterogeneity in grain size, the wettability of the laminae can also differ. The laminae can contain different minerals with different wetting characteristics, and wettability can be affected by adsorption of hydrocarbons to the grain surface. In this paper we focus on the effects of wettability on the entrapment. We describe a procedure that allows the reader to quantify the trapped oil saturation depending on absolute permeability, relative permeability, and capillary pressure curves of the foreset laminae, on the basis of a simplified crossbed geometry. The example calculations show the sensitivity of various parameters with respect to the magnitude of trapping.

Introduction

The importance of capillary entrapment in small-scale heterogeneities during waterflooding and EOR projects is generally recognized.[1-3] A typical heterogeneous facies is the crossbedded sandstone (**Fig. 1**), which is associated with fluvial and deltaic deposits. Crossbedded reservoirs can be very fine to coarse grained and are generally moderately well sorted.

Crossbed sets consist of foresets and bottomsets. The foresets consist of alternating layers of fine-grained and coarse-grained material with sharp boundaries. The bottomset consists of fine-grained material comparable with the fine-grained foreset laminae. Typically, the average grain size of the fine-grained and coarse-grained laminae differs by a factor 1.5. The coarse-grained laminae are generally more poorly sorted.[4] **Table 1** gives some typical length scales of crossbed sets that were obtained from outcrop studies at a fluvial deposit in Spain.[4]

Oil displacement from crossbed sets has received broad attention. Ringrose *et al.*[5] studied the effects of crosslayer flow and along-layer flow by numerical simulation. They determined oil pseudorelative permeability curves on the basis of simulation results. Pickup *et al.*[6,7] introduced tensorial effects for one-phase and two-phase flow. The papers show the complexity involved in the quantification of trapped oil in crossbedded structures.

In this paper, we focus on the effects of heterogeneities in wettability and pore-structure on the residual oil saturation (ROS) in crossbedded reservoirs. To this end, we derived simple analytical formulas relating the ROS to the dimensionless capillary number. These formulas clearly demonstrate the effects of sorting, wettability, and scale. We validated the results through scaled laboratory experiments. Although the formulas were derived for simplified geometrical models, they allow the reader to obtain a quick estimate of the importance of trapping under specific field conditions.

Wettability in Crossbedded Reservoirs

Apart from the heterogeneity in pore geometry, crossbed sets may also show variations in the wettability of the laminae. One of the causes for wettability heterogeneities can be variations in the mineralogy of the different laminae. Hartkamp-Bakker[4] reports variations with respect to the amount of quartz, kaolinite, and anhydrite in crossbedded fluvial sandstones. Robin *et al.*[8] found that quartz, feldspar, and illite remain preferentially water-wet, while kaolinite booklets were found to be oil-wet. They also reported that particle size can influence wettability.

Wettability in crossbed sets can also be influenced by adsorption of hydrocarbon fractions (asphaltenes and resins) to the rock matrix. When oil migrates into a water-wet reservoir rock, it will occupy the largest pores, while the smaller pores remain filled by water because of insufficient capillary pressure. In time, oil-filled pores may become oil-wet by adsorption of hydrocarbons.[9-11] This complicated ageing process depends on brine composition (pH, salinity), oil composition (asphaltenes, resins), and mineral composition.

In the literature, the terminology to describe the different types of wettability is sometimes confusing. We follow the definitions used by Anderson.[12]

Fully Water-Wet. A thin film of water prevents contact between the hydrocarbon phase and the grain surface.

Fully Oil-Wet. The rock matrix is covered by a thin oil film at all times.

Intermediate Wet. The oil/water interface makes a distinct contact angle with the rock matrix.

Fractionally Wet. The internal rock surface consists of a random distribution of water-wet and oil-wet sections. This state of wettability can occur when the matrix is composed of different minerals that may differ in wetting characteristics or because of selective adsorption to random parts of the rock matrix.

Mixed-Wet. The larger pores have become oil-wet owing to adsorption of hydrocarbons. The small pores have remained water-wet.

Trapping Conditions at Heterogeneity Boundaries

Capillary entrapment at heterogeneity boundaries is a well-known phenomenon. Recently the conditions at a heterogeneity boundary were clearly documented.[13] When the saturations are greater than residual on both sides of the boundary, continuity in capillary pressure is required. If, however, the saturation of one of the phases is residual at either side of the boundary (e.g., $S_w = S_{wr}$ or $S_o = S_{or}$), the capillary pressure does not need to be continuous at the boundary. In the next section, we apply the conditions at heterogeneity boundaries to a simplified model of a crossbed set. In the process, we derive formulas that quantify the fraction of oil that is trapped permanently.

Physical Modeling of Capillary Entrapment in Crossbedded Reservoirs

Apart from the flow properties of the laminae, the geometry of the crossbed set and the pressure gradient relative to the geometry play an integral role in capillary entrapment in crossbedded reservoirs. For an exact treatment of capillary entrapment in these reservoirs, we need to model heterogeneity on lamina scale and resort to numerical simulation to determine the capillary trapped oil. This procedure is time consuming and may lead to numerical problems. In addition, for practical applications, the detailed information necessary to justify this approach is generally not available. We chose to derive simple analytical formulas with which the extent of trapping can be estimated. We model the crossbed set as a box-like structure with a specific length, width, and height (Fig. 1). In our model, the foresets consist of alternating fine- and coarse-grained laminae, while we assume that the composition and flow properties of the bottomsets are similar to those of the fine-grained foreset laminae (the latter assumption is not strictly necessary, but simplifies the final result). Capillary entrapment in this model depends on the direc-

Original SPE manuscript received for review Oct. 17, 1995. Revised manuscript received March 15, 1996. Paper peer approved March 19, 1996. Paper (SPE 30782) first presented at the 1995 SPE Annual Technical Conference and Exhibition held in Dallas, Oct. 22-25.

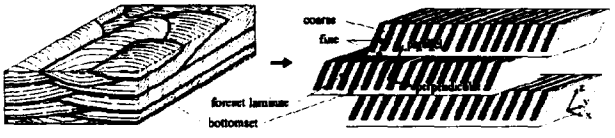

Fig. 1—On the right (from Ref. 2), a 3D model of vertically stacked trough crossbeds with distinctive foreset and bottomset facies. On the left, the schematized model. The crossbed sets are characterized as box-like structures with a specific length, height, and width. The foreset and bottomset laminae within this box-like structure have characteristic dimensions.

tion of the pressure gradient in the reservoir relative to the orientation of the box. We discuss two cases.

Flow perpendicular to foreset laminae. The pressure gradient is in the x direction.

Flow parallel to foreset laminae. The pressure gradient can be in the y or the z direction.

We assume that these two situations are close to the worst- and best-case scenarios with respect to oil entrapment. In the following paragraphs, we derive the analytical formulas that relate trapped oil saturation to the capillary number and the endpoint relative permeability of the water phase. In these formulas we disregard gravity. The results are listed in **Table 2.**

Flow Perpendicular to Foreset Laminae. We apply the previously mentioned conditions at a heterogeneity boundary to a situation where the pressure gradient of the injected water phase is perpendicular to the laminae of the foreset. **Fig. 2** shows the capillary pressure curves that may apply to the coarse-grained and fine-grained laminae of a water-wet foreset. We label the lamina type with the lowest capillary pressure at $S_w = 1 - S_{or}$ with the subscript 1 and the other lamina type with the subscript 2. Initially, the laminae are in capillary equilibrium. Hence, the saturation in the laminae depends on the capillary pressure. When the laminae are flooded with water, capillary continuity between the downstream boundary of Lamina 1 and the upstream boundary of Lamina 2 will be maintained until the ROS of Lamina 2 is reached. At this point in time, the water saturation at the downstream boundary of Lamina 1 can no longer increase. We define this maximum water saturation at the downstream boundary of Lamina 1, which results from the capillary equilibrium condition when the saturation at the upstream boundary of Lamina 2 tends to $1 - S_{or}$, as $S_{w,d}$.

We now consider the water saturation within Lamina 1 after extensive flooding. For the water phase, we can write Darcy's law:

$$v_w = -\frac{k_1 k_{rw1}}{\mu_w}\frac{dp_w}{dx}. \quad \ldots\ldots\ldots\ldots\ldots\ldots\ldots\ldots\ldots\ldots (1)$$

Upstream of the downstream boundary of Lamina 1, the capillary pressure is continuous as long as both phases at more than their residual saturation. Furthermore, v_o is zero, which implies that p_o is constant where $S_o > S_{or}$. Therefore, $dp_w/dx = -(dP_c/dx)$. We rewrite Eq. 1 as

$$v_w = \frac{k_1 k_{rw1}}{\mu_w}\frac{\partial P_c}{\partial x} = \frac{k_1 k_{rw1}}{\mu_w}\frac{dP_c}{dS_w}\frac{dS_w}{dx}. \quad \ldots\ldots\ldots\ldots\ldots\ldots\ldots\ldots (2)$$

We can write Eq. 2 in a dimensionless form with $P_c = \sigma_{ow}\sqrt{\phi/k}J(S_w)$:

$$1 = N_{cv,x} k_{rw1} J' \frac{dS_w}{dx_D}, \quad \ldots\ldots\ldots\ldots\ldots\ldots\ldots\ldots\ldots\ldots (3)$$

$$\text{where } N_{cv,x} = \frac{\sqrt{k_1\phi_1}\,\sigma_{ow}}{\mu_w v_w h_1} \quad \ldots\ldots\ldots\ldots\ldots\ldots\ldots\ldots\ldots\ldots (4)$$

$$\text{and } x_D = \frac{x}{h_1}. \quad \ldots\ldots\ldots\ldots\ldots\ldots\ldots\ldots\ldots\ldots\ldots\ldots (5)$$

$N_{cv,x}$ is the dimensionless capillary number perpendicular to the foreset laminae, J' is the derivative of the Leverett-J function with respect to water saturation, x_D is the dimensionless distance perpendicular to the laminae, and h_1 is the thickness of the laminae in which oil is trapped. Integration of Eq. 2 leads to the following expression for the capillary number as a function of the water saturation $S_{w,u}$ at the upstream boundary of Lamina 1:

$$N_{cv,x}(S_{w,u}) = -\frac{1}{\int_{S_{w,d}}^{S_{w,u}} J'(\omega)k_{rw}(\omega)d\omega}. \quad \ldots\ldots\ldots\ldots\ldots\ldots (6)$$

From Eq. 6, the capillary number can be calculated for $1 - S_{or} < S_{w,u} < S_{w,d}$. Depending on the wettability, the Leverett-J function can have a definite endpoint when the oil saturation tends to the residual saturation. In these cases, ROS can be reached between the upstream and the downstream boundaries of Layer 1 at dimensionless distance α from the downstream boundary. In this case, the following expression applies:

$$N_{cv,x}(\alpha) = -\frac{\alpha}{\int_{S_{w,d}}^{1-S_{or1}} J'(\omega)k_{rw}(\omega)d\omega}. \quad \ldots\ldots\ldots\ldots\ldots\ldots (7)$$

Eqs. 6 and 7 describe the capillary number from ∞ to 0. Straightforward calculus enables us to find similar expressions for the permanently trapped oil $S_{o,i}$ and the effective water permeability at $S_w = 1 - S_{o,i}$. The relevant formulas are listed in Table 2, Column A. To simplify the formulas, we assume that the bottomsets have no conductivity nor volume. The formulas in Table 2 involve simple numerical integration and can be applied for specific field conditions. Example calculations follow later.

Flow Parallel to Foreset Laminae. Here, we look at flow parallel to the foreset laminae. In this case, oil may be permanently trapped against the bottomset laminae. The assumption that the bottomset has the same characteristics as the fine-grained foreset laminae implies that oil can only be trapped in the coarse-grained laminae, which we label with the subscript 1. After extensive flooding, the remaining oil in Lamina 1 will be stationary. We copy Eq. 2 and apply it to parallel flow of water in Lamina 1:

$$v_{w1} = \frac{k_1 k_{rw1}}{\mu_w}\frac{dP_c}{dS_w}\frac{dS_w}{dy}. \quad \ldots\ldots\ldots\ldots\ldots\ldots\ldots\ldots\ldots\ldots (8)$$

For the average parallel flow velocity of the water phase, we write

$$v_w = \frac{h_1 v_{w1} + h_2 v_{w2}}{h_1 + h_2}. \quad \ldots\ldots\ldots\ldots\ldots\ldots\ldots\ldots\ldots\ldots (9)$$

We now use the following equilibrium approximation, where we disregard viscous forces perpendicular to the laminae:

$$\left(\frac{dp_w}{dy}\right)_1 = \left(\frac{dp_w}{dy}\right)_2 \quad \ldots\ldots\ldots\ldots\ldots\ldots\ldots\ldots\ldots\ldots (10)$$

(i.e., the pressure gradient in Lamina 1 equals the pressure gradient in Lamina 2) to describe the flow in Layer 2 in terms of the flow in Layer 1:

$$v_{w2} = \frac{k_2 k^*_{rw2}}{k_1 k_{rw1}} v_{w1}, \quad \ldots\ldots\ldots\ldots\ldots\ldots\ldots\ldots\ldots\ldots (11)$$

TABLE 1—STATISTICS OF TROUGH CROSSBED SETS

Length, m		2–20
Width, m		0.5–5
Thickness, m		0.14–0.4
Thickness coarse foreset laminae, m	h_1	0.004–0.015
Thickness fine foreset laminae, m	h_2	0.002–0.01
Thickness bottomset, m		0.01–0.1

TABLE 2—SUMMARY OF FORMULAS FOR QUANTIFICATION OF TRAPPED OIL

	A: Perpendicular			B: Parallel		
	$k_{e,x} =$	$\frac{(1+\lambda)}{1+\frac{\lambda}{\tau}} k_1$	1	$k_{e,y} =$	$\frac{1+\lambda\tau}{1+\lambda} k_1$	1
	$N_{cv,x} =$	$\frac{\sqrt{k_1\phi_1}\sigma_{ow}}{\mu_w v_w h_1}$	2	$N_{cv,y} =$	$\frac{\sqrt{k_1\phi_1}\sigma_{ow}}{\mu_w v_w b}$	2
	$v_{w,x} =$	$\frac{\sqrt{k_1\phi_1}\sigma_{ow}}{\mu_w h_1 N_{cv,x}}$	3	$v_{w,y} =$	$\frac{\sqrt{k_1\phi_1}\sigma_{ow}}{\mu_w b N_{cv,y}}$	3
	$\left\lvert\frac{dp}{dx}\right\rvert =$	$\frac{v_{w,x}\mu_w}{k_{e,x}k_{rw,x}}$	4	$\left\lvert\frac{dp}{dy}\right\rvert =$	$\frac{v_{w,y}\mu_w}{k_{e,y}k_{rw,y}}$	4
	$S_{w,d} =$	S_{w1} at $J_1 = J_2(1-S_{or2})$	5	$S_{w,d} =$	S_{w1} at $J_1 = J_2(1-S_{or2})$	5
$S_{w,u} \in (S_{w,d}, 1-S_{or1})$	$N_{cv,x}(S_{w,u}) =$	$\frac{-1}{\int_{S_{w,d}}^{S_{w,u}} J_1'(\omega)k_{rw1}(\omega)d\omega}$	6	$N_{cv,y}(S_{w,u}) =$	$\frac{-(1+\lambda)}{\int_{S_{w,d}}^{S_{w,u}} \left(k_{rw1}(\omega)+\tau\lambda k^*_{rw2}\right)J_1'(\omega)d\omega}$	6
	$S_{o,ix}(S_{w,u}) =$	$\frac{1+\lambda S_{or2}}{1+\lambda} + \cdots$ $\cdots + \frac{N_{cv,x}(S_{w,u})\int_{S_{w,d}}^{S_{w,u}} J_1'(\omega)k_{rw1}(\omega)\omega d\omega}{1+\lambda}$	7	$S_{o,iy}(S_{w,u}) =$	$\frac{1+\lambda S_{or2}}{1+\lambda} + \cdots$ $\cdots + \frac{N_{cv,x}(S_{w,u})\int_{S_{w,d}}^{S_{w,u}} (k_{rw1}(\omega)+\tau\lambda k^*_{rw2})J_1'(\omega)\omega d\omega}{(1+\lambda)^2}$	7
	$k_{rw,x}(S_{w,u}) =$	$\frac{1+\frac{\lambda}{\tau}}{N_{cv,x}(S_{w,u})(J_1(S_{w,d})-J_1(S_{w,u}))+\frac{\lambda}{\tau k^*_{rw2}}}$	8	$k_{rw,y}(S_{w,u}) =$	$\frac{1+\lambda}{(1+\lambda\tau)N_{cv,y}(S_{w,u})(J_1(S_{w,d})-J_1(S_{w,u}))}$	8
$\alpha \in (1,0)$	$N_{cv,x}(\alpha) =$	$\frac{-\alpha}{\int_{S_{w,d}}^{1-S_{or1}} J_1'(\omega)k_{rw1}(\omega)d\omega}$	9	$N_{cv,y}(\alpha) =$	$\frac{-\alpha(1+\lambda)}{\int_{S_{w,d}}^{1-S_{or1}} \left(k_{rw1}(\omega)+\tau\lambda k^*_{rw2}\right)J_1'(\omega)d\omega}$	9
	$S_{o,ix}(\alpha) =$	$\frac{\alpha(1-S_{or1})+S_{or1}+\lambda S_{or2}}{1+\lambda} + \cdots$ $\cdots + \frac{N_{cv,x}(\alpha)\int_{S_{w,d}}^{1-S_{or1}} J_1'(\omega)k_{rw1}(\omega)\omega d\omega}{1+\lambda}$	10	$S_{o,iy}(\alpha) =$	$\frac{\alpha(1-S_{or1})+S_{or1}+\lambda S_{or2}}{1+\lambda} + \cdots$ $\cdots + \frac{N_{cv,x}(\alpha)\int_{S_{w,d}}^{1-S_{or1}} (k_{rw1}(\omega)+\tau\lambda k^*_{rw2})J_1'(\omega)\omega d\omega}{(1+\lambda)^2}$	10
	$k_{rw,x}(\alpha) =$	$\frac{1+\frac{\lambda}{\tau}}{\frac{(1-\alpha)}{k^*_{rw1}}+N_{cv,x}(\alpha)(J_1(S_{w,d})-J_1(1-S_{or}))+\frac{\lambda}{\tau k^*_{rw2}}}$	11	$k_{rw,y}(\alpha) =$	$\frac{\left[\left(\frac{1-\alpha}{k^*_{rw1}+\tau\lambda k^*_{rw2}}+\frac{N_{cv,y}(\alpha)(J_1(S_{w,d})-J_1(1-S_{or}))}{1+\lambda}\right)\right]^{-1}}{(1+\lambda\tau)}$	11

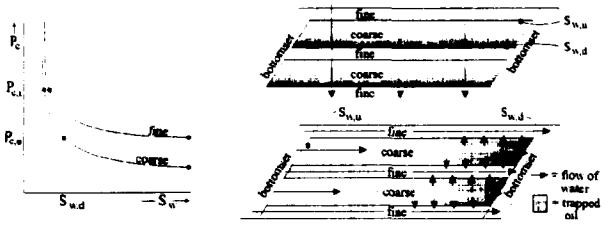

Fig. 2—Capillary entrapment perpendicular and parallel to the foreset laminae. On the left, capillary pressure curves for coarse-grained and fine-grained water-wet laminae. Indicated are the initial capillary pressure and the capillary pressure at which oil is trapped at the downstream boundary of the coarse-grained laminae. On the right, the model for flow perpendicular (top) and parallel (bottom) to the foreset laminae. The arrows indicate the flow direction of the water phase.

where k^*_{rw2} is the relative water permeability at the ROS in Layer 2. Fig. 2 shows a schematized drawing of capillary entrapment during parallel flow. In the area where the oil is trapped, the water phase is diverted to the surrounding laminae. We see that there is no continuity in capillary pressure at the boundary between the fine-grained and coarse-grained foreset laminae. Yet, along this boundary, the saturation in Lamina 1 may vary between $(1-S_{or})$ and $S_{w,d}$. We note that this situation is in agreement with the boundary conditions stated by Van Duijn *et al.*[14] We combine Eqs. 8, 9, and 11:

$$\frac{1+\lambda}{1+\frac{\lambda\tau k^*_{rw2}}{k_{rw1}}} = \frac{k_1 k_{rw1}}{v_w \mu_w}\frac{dP_c}{dS_w}\frac{dS_w}{dy}, \quad \ldots\ldots\ldots\ldots\ldots\ldots (12)$$

where $\lambda = h_2/h_1$ and $\tau = k_2/k_1$. We now write Eq. 12 in a dimensionless form:

$$1 = \frac{N_{cv,y}}{1+\lambda}\left(k_{rw1} + \lambda\tau k^*_{rw2}\right)J'\frac{dS_w}{dy_D}, \quad \ldots\ldots\ldots\ldots\ldots\ldots (13)$$

where $N_{cv,y} = \dfrac{\sqrt{k_1\phi_1}\,\sigma_{ow}}{\mu_w v_w b}$ ..... (14)

and $y_D = \dfrac{y}{b}$. ..... (15)

$N_{cv,y}$ is the dimensionless capillary number that applies parallel to the foreset laminae, J is the Leverett-J function, y_D is the dimensionless distance perpendicular to the laminae, and b represents the width of the foreset lamina. Integration of Eq. 13 leads to the following expression for the capillary number as a function of the water saturation $S_{w,u}$ at the upstream boundary of Lamina 1:

$$N_{cv,y}(S_{w,u}) = -\frac{(1+\lambda)}{\int_{S_{w,d}}^{S_{w,u}} \left[k_{rw1}(\omega) + \tau\lambda k^*_{rw2}\right]J'(\omega)d\omega}. \quad \ldots\ldots (16)$$

Again, we may need to apply a factor α to describe the full range of capillary numbers in the case where the Leverett-J function has a definite endpoint at $S_w = 1 - S_{or}$. When the ROS is reached at a dimensionless distance α from the downstream boundary of Lamina 1, the capillary number is

$$N_{cv,y}(\alpha) = -\frac{\alpha(1+\lambda)}{\int_{S_{w,d}}^{1-S_{or1}} \left[k_{rw1}(\omega) + \tau\lambda k^*_{rw2}\right]J'(\omega)d\omega}. \quad \ldots\ldots (17)$$

Expressions for the permanently trapped oil $S_{o,i}$ and the effective water permeability at $S = 1 - S_{o,i}$, which follow from Eq. 17, are listed in Table 2, Column B. For simplicity, we assume that the bottomset acts as a heterogeneity boundary with infinite conductivity and no volume. Example calculations follow later.

Experimental Verification of Trapping at a Heterogeneity Boundary

We performed glass-bead experiments[15] to validate the trapping mechanism during perpendicular flow. The experiments were performed with a slab-type model (length = 0.5 m, width = 0.16 m, height = 0.01 m), in which we measured the water saturation by means of the microwave absorption technique.[16-21] We filled the upstream part of the model with coarse-grained and the downstream part with fine-grained glass beads. We measured the trapping of decane against the grain-size discontinuity during flooding with water. **Fig. 3,** on the left, shows the saturation profile plotted vs. the distance from the heterogeneity at four different flow velocities. To plot these data in a dimensionless form, we rewrite Eq. 3:

$$\frac{x_D}{N_{cv,x}} = \int_{S_{w,d}}^{S_{w,x_D}} k_{rw1}(\omega)J'(\omega)d\omega. \quad \ldots\ldots\ldots\ldots\ldots\ldots (18)$$

In Fig. 3, on the right, we plot the four saturation curves vs. $x_D/N_{cv,x}$. The figure shows a good match between the four different curves, indicating that the scaling procedure is correct.

Results and Discussion

We applied the derived formulas to a crossbedded structure defined in **Table 3.** The parameters are based on modeling work done by Hartkamp-Bakker[4] and Ringrose *et al.*[5] The relative permeabilities and the Leverett-J functions we used are based on the Brooks-Corey[22] model, which describes these curves as a function of the sorting factor and the threshold capillary pressure at $S_w = 1$.

In **Fig. 4,** permanently trapped oil is plotted vs. the perpendicular and the parallel (in the width direction) macroscopic pressure gradient. To show the sensitivity of some of the parameters involved, we changed one parameter in each of the plots.

In Fig. 4a, we see the effect of the lamina thickness ratio, λ. This ratio is changed from 1 to 0.5 by increasing the thickness of the coarse-grained laminae. As a result, the capillary number (Eq. A2 in Table 2)

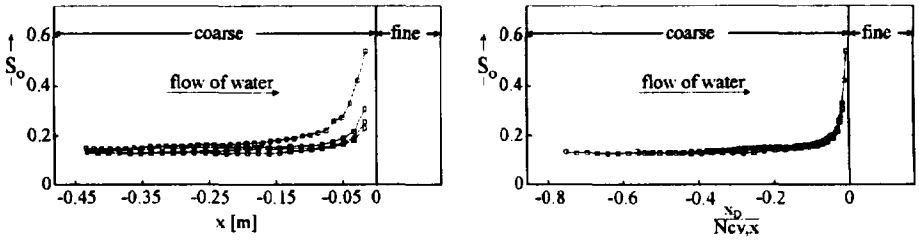

Fig. 3—Experimental data on the trapping of oil in a coarse-grained, water-wet lamina. On the left, saturation plotted vs. distance for four different flow rates. On the right, saturation plotted vs. the dimensionless distance divided by the capillary number. We see that the curves for the four different flow rates overlap, indicating that correct scaling was applied.

TABLE 3—CROSSBED CHARACTERISTICS USED IN EXAMPLE CALCULATIONS

	Lamina 1	Lamina 2
Vertical width of laminae, m	2.0	
Horizontal width of laminae, b, m	0.5	
Thickness of laminae, h, m	0.01	0.01
Permeability in laminae, k, md	200	50
Porosity, ϕ	0.3	0.3
ROS, S_{or}	0.2	0.2
Residual water saturation, S_{wr}	0.15	0.15
Sorting factor, ϵ	1.5	1.5
$J(S_w=1)$, C	0.5	0.5
Interfacial tension, σ_{ow}, N/m	0.03	
Viscosity, water phase, μ_w, Pa·s	0.001	
Relative water permeability, k_{rw}	$k_{rw} = S_w^{(2+3\epsilon)/\epsilon}$	
Relative oil permeability, k_{ro},	$k_{ro} = (1 - S_w)^2(1 - S_w^{(2+\epsilon)/\epsilon})$	
Leverett-J function, J	$J = CS_w^{-1/\epsilon}$	

perpendicular to the laminae decreases and the curve for perpendicular flow shifts to the left. Another effect is that the volume in which oil can be trapped is increased; hence, more oil can potentially be trapped.

Fig. 4b demonstrates the effect of the permeability contrast, τ. This contrast is changed from $^1/_4$ to $^1/_8$ by increasing the permeability of the coarse-grained laminae. Both the perpendicular and parallel capillary number increase, resulting in a shift of both curves to the right. Furthermore, the water saturation at the downstream boundary of the trapping layer decreases, resulting in a higher maximum trapping.

In Fig. 4c, we increased the width of the foreset laminae by a factor of 2. This results in an increased capillary number parallel to the laminae. Less oil is permanently trapped under the same parallel pressure gradient. Perpendicular trapping is not affected.

In Fig. 4d, we increased the sorting factor for the coarse-grained laminae from 1.5 to 3. The water saturation $S_{w,d}$ at the downstream boundary decreases; therefore, more oil can potentially be trapped. In addition the gradient J' of the Leverett-J function becomes less steep, resulting in a shift to the left for both curves.

Effects of Wettability. We have seen that the conditions at the heterogeneity boundary play an important role in the trapping mechanism. Wettability has a direct effect on the capillary pressure curves and therefore on the saturation at the downstream boundary of the trapping laminae. Alternating water-wet and oil-wet laminae, for instance, may lead to severe trapping. However, this situation is probably not very realistic. Under fully oil-wet conditions, the large gradient in the capillary pressure curves close to ROS's will lead to a very low fraction of permanently trapped oil (however, delay in production will occur). One other important aspect is that, under oil-wet conditions, oil is potentially trapped in the fine-grained laminae, whereas under water-wet conditions trapping takes place in coarse-grained laminae. In our simplified model, we clearly see the implications; the fine-grained laminae form a continuous path through the crossbedded reservoir. Therefore, the length scale involved in the capillary number is many times larger than the length scales in the crossbed set, and no significant permanent trapping will take place.

The effect of fractional wettability is shown in Figs. 4e and 4f. We modeled mixed wettability by lowering the constant C in the Brooks-Corey capillary pressure model. This constant represents the Leverett-J value at $S_w = 1$. We disregarded the effects of mixed wettability on the relative permeability curves. In Fig. 4e, the constant C of the coarse-grained laminae is changed from 0.5 to 0.25. The figure shows that more oil can potentially be trapped. In Fig. 4f, we changed the constant C of the fine grained laminae from 0.5 to 0.3. As could be expected, trapping becomes less severe.

Conclusions

1. Wettability plays an important role in trapping in crossbed sets.
2. We derived simple expressions with which the magnitude of capillary entrapment can be estimated.
3. The derived expressions clearly show the sensitivity of capillary trapped oil to wetting, sorting, lamina permeability, and the dimensions of crossbed sets.

Nomenclature

b = width of a foreset lamina, L, m
C = constant in the Brooks-Corey model representing the Leverett-J value at $S_w = 1$
$|dp/dx|$ = macroscopic pressure gradient, $1/Lt^2$, Pa/m
h = thickness of a foreset lamina, L, m
J = Leverett-J function
J' = derivative of the Leverett-J function with respect to water saturation
k = permeability, L^2, m^2
k_r = relative permeability
L = thickness, length or width, L, m
N = dimensionless capillary number
p = pressure, m/Lt^2, Pa
P_c = capillary pressure, m/Lt^2, Pa
S = saturation
v = Darcy velocity, L/t, m/s
x = distance perpendicular to the foreset laminae, L, m
y = distance parallel to the foreset laminae, L, m
α = dimensionless distance from a boundary to the location where $S_o = S_{or}$
ϵ = sorting factor
θ = contact angle
λ = ratio of laminae thicknesses h_2/h_1
μ = viscosity, m/Lt, Pa·s
τ = ratio of permeabilities k_2/k_1
ϕ = porosity, fraction
ω = integration parameter

Subscripts

cv = capillary over viscous forces
d = at the downstream boundary of Lamina 1
e = effective
i = permanently trapped
n = normalized
o = oil
or = oil residual
ow = between oil and water
rw = relative, water
u = at the upstream boundary of Lamina 1
w = water
wr = water residual
x = the direction perpendicular to the foreset laminae
y = the width direction parallel to the foreset laminae
z = the height direction parallel to the foreset laminae
σ = interfacial tension, m/t^2, N/m
1 = the lamina type of the foreset in which oil is trapped
2 = the lamina type of the foreset in which oil is not permanently trapped

Superscript

* = at the ROS

Acknowledgments

This study is funded in part by TNO. We thank the technical and electronics staff of the Dietz-laboratory, in particular A. Hoving and L. Vogt, for their assistance during the design and construction of the experimental setups. We thank Halliburton for the supply of resin-coated sands.

References

1. Kortekaas, T.: "Water/Oil Displacement in Crossbedded Reservoir Zones," *SPEJ* (Dec. 1985) 917–926.

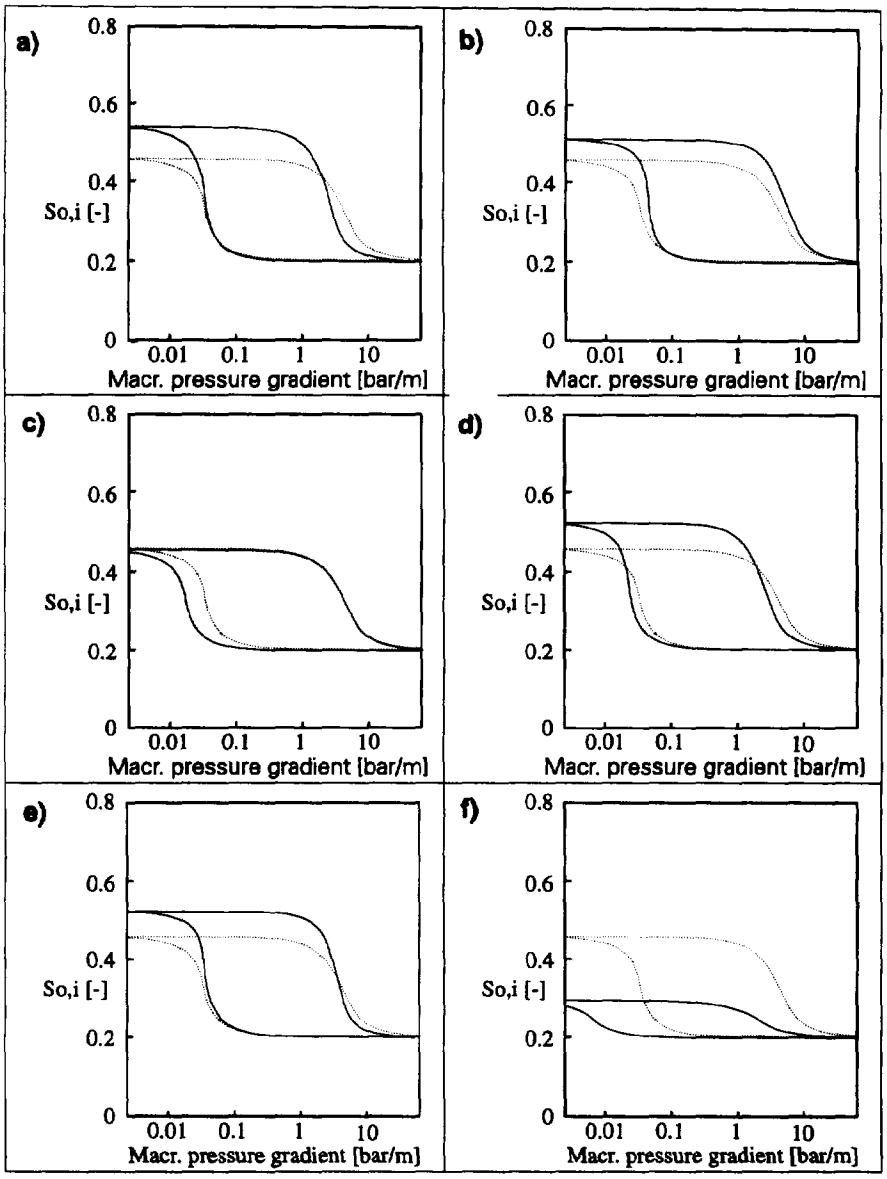

Fig. 4—Example calculations showing the sensitivity of some of the parameters involved in trapping. The dotted curves represent the "base" case for perpendicular (highest) and parallel (lowest) flow. a) The effect of decreasing the ratio of lamina thickness from 1 to 0.5. b) The effect of decreasing the permeability ratio from $^1/_4$ to $^1/_8$. c) The effect of increasing the width of the foresets by a factor of 2. d) The effect of increasing the sorting factor of the coarse-grained laminae by a factor of 2. e) The effect of mixed wettability in the coarse-grained laminae. f) The effect of mixed wettability in the fine-grained laminae.

2. Weber, K.: "How Heterogeneity Affects Oil Recovery," *Reservoir Characterization*, L. Lake and H. Carroll (eds.), Academic Press Inc., Orlando, FL (Sept. 1994) 487–544.
3. Morrow, N.: "Small-Scale Packing Heterogeneity in Porous Sedimentary Rocks," *AAPG Bulletin* (1971) **55**(3), 514–522.
4. Hartkamp-Bakker, C.: "Permeability Heterogeneity in Crossbedded Sandstones—Impact on Water/Oil Displacement in Fluvial Reservoirs," PhD dissertation, Delft U. of Technology (Sept. 1993).
5. Ringrose, P. *et al.*: "Immiscible Flow Behavior in Laminated and Crossbedded Sandstones," *J. Pet. Science & Engineering* (Sept. 1993) 103–124.
6. Pickup, G. and Sorbie, K.: "Development and Application of a New Two-Phase Scaleup Method on Tensor Permeabilities," in *Proc.*, SPE Annual Technical Conference and Exhibition, New Orleans, LA (Sept. 1994) 217–230.
7. Pickup, G. *et al.*: "Geology, Geometry and Effective Flow," in *Proc.*, SPE Annual Technical Conference and Exhibition, New Orleans, LA (Sept. 1994) 93–104.
8. Robin, M., Rosenberg, E., and Fassi-Fihri, O.: "Wettability Studies at the Pore Level: A New Approach by Use of Cry-Sem," *SPEFE* (March 1995) 11–19.
9. Hirasaki, G.: "Wettability: Fundamentals and Surface Forces," in *Proc.*, SPE/DOE Enhanced Oil Recovery Symposium, Tulsa, OK (April 1988).
10. Morrow, N., Lim, H., and Ward, J.: "Effect of Crude-Oil-Induced Wettability Changes on Oil Recovery," *SPEFE* (Feb. 1986) 89–103.
11. Crocker, M. and Marchin, L.: "Wettability and Adsorption Characteristics of Crude-Oil Asphaltene and Polar Fractions," *JPT* (1988) 470–474.
12. Anderson, W.: "Wettability Literature Survey—Part 1: Rock/Oil/Brine Interactions and the Effects of Core Handling on Wettability," *JPT* (Oct. 1986) 1125–1145.
13. Van Duijn, Molenaar, J., and de Neef, M.: "The Effect of Capillary Forces on Immiscible Two-Phase Flow in Heterogeneous Porous Media," Technical Report 94-103 ISSN 0922-5641, Faculty of Technical Mathematics & Informatics, Delft U. of Technology (1994).

14. van Duijn, C., Molenaar, J., and de Neef, M.: "The Effect of Capillary Forces on Immiscible Two-Phase Flow in Heterogeneous Porous Media," *Transport in Porous Media* (1995) **21**(1), 71–93.
15. van Lingen, P., Bruining, J., and van Kruijsdijk, C.: "Capillary Entrapment Due to Small-Scale Wettability Heterogeneities," in *Reservoir Engineering Proc.*, SPE Annual Technical Conference and Exhibition, Dallas, TX (Oct. 1995).
16. Hanssen, J.: "Foam as a Gas-Blocking Agent in Petroleum Reservoirs II: Mechanisms of Gas Blockage by Foams," *J. Pet. Science & Engineering* (Oct. 1993) 135–156.
17. Bauer, K. *et al.*: "The Formation and Following Up of the Fluid Saturation in the Rock Model by Secondary and Tertiary Oil Displacement Processes," in *Proc.*, Third Symposium on Mining Chemistry, Siófok, Hungary (Oct. 1990).
18. Tichy-Rács, A. *et al.*: "Measurement of Water Content in Oil Reservoir Rocks by Microwave Absorption," in *Proc.*, Microwaves and Optoelectronics (MIOP), Rhein-Main-Halle, Germany (March 1988).
19. Sharma, D.: "Kinetics of Oil Bank Formation," PhD dissertation, U. of California, Berkeley (Dec. 1987).
20. Haskin, H. and Davis, L.: "A Comparison of Laboratory Linear and Pattern Flow Chemical Floods Using a Volumetric Linear Scaling Concept for Oil Saturation Distributions," in *Proc.*, SPE-AIME Annual Fall Technical Conference and Exhibition, San Antonio, TX (Oct. 1981).
21. Parsons, R.: "Microwave Attenuation—A New Tool for Monitoring Saturations in Laboratory Flooding Experiments," *SPEJ* (Oct. 1975) 302–310.
22. Brooks, R. and Corey, A.: "Hydraulic Properties of Porous Media," Technical Report, Colorado State U. (1964). Hydrology papers.

SI Metric Conversion Factors

bar ×1.0*	E+05 = Pa
cp ×1.0*	E−03 = Pa·s
dyne/cm ×1.0*	E+00 = mN/m
ft ×3.048*	E−01 = m
md ×9.869 233	E−04 = μm^2

*Conversion factor is exact.

SPERE

Paul van Lingen is a PhD student from the Dietz laboratory at the Faculty of Mining & Petroleum Engineering, Delft U. of Technology. The topic of his study is capillary entrapment in small-scale heterogeneities during immiscible flooding. He holds an MS degree in mining and petroleum engineering. **Hans Bruining** is the head of the Dietz laboratory for reservoir engineering at Delft U. of Technology. His interest is in theoretical and experimental modeling of complex flow problems in heterogeneous porous media with applications to thermal recovery, underground coal gasification, improved recovery/production with polymers, and DNAPL spreading. He holds a PhD degree in physical chemistry from the U. of Amsterdam. **C.P.J.W. van Kruijsdijk** holds the chair of reservoir engineering at Delft U. of Technology, in combination with a position at the Inst. of Applied Geoscience. Previously, he was with Shell Intl. E&P B.V. in The Netherlands from 1985 to 1989 and with Shell Canada Ltd. in Calgary from 1989 to 1993. He holds an MS degree in physics from U. Eindhoven in The Netherlands. van Kruijsdijk, currently a Review Chairman for *SPE Reservoir Engineering*, has served on the Editorial Review Committee since 1991. He is a current member of an Annual Meeting Technical Committee and served as a 1994–95 member of the Forum Series Committee and the European Formation Damage Symposium Program Committee.


van Lingen


Bruining


van Kruijsdijk